NASA Contractor Report 198490

Coupled Mixed-Field Laminate Theory and Finite Element for Smart Piezoelectric Composite Shell Structures

Dimitris A. Saravanos
Ohio Aerospace Institute
Cleveland, Ohio

June 1996

COUPLED MIXED-FIELD LAMINATE THEORY AND FINITE ELEMENT FOR SMART PIEZOELECTRIC COMPOSITE SHELL STRUCTURES

Dimitris A. Saravanos
Senior Research Associate

Ohio Aerospace Institute
Structural Mechanics Branch
NASA Lewis Research Center
21000 Brookpark Rd., MS 49-8
Cleveland, Ohio 44135

Abstract

Mechanics for the analysis of laminated composite shells with piezoelectric actuators and sensors are presented. A new mixed-field laminate theory for piezoelectric shells is formulated in curvilinear coordinates which combines single-layer assumptions for the displacements and a layerwise representation for the electric potential. The resultant coupled governing equations for curvilinear piezoelectric laminates are described. Structural mechanics are subsequently developed and an 8-node finite-element is formulated for the static and dynamic analysis of adaptive composite structures of general laminations containing piezoelectric layers. Evaluations of the method and comparisons with reported results are presented for laminated piezoelectric-composite plates, a closed cylindrical shell with a continuous piezoceramic layer and a laminated composite semi-circular cantilever shell with discrete cylindrical piezoelectric actuators and/or sensors.

1. Introduction

Smart composite laminates and adaptive composite structures with embedded piezoelectric sensors and actuators seem to combine some of the superior mechanical properties of composites with the additional capabilities to sense deformations and stress states and to adapt their response accordingly. Consequently, such novel and structures are receiving substantial research interest. Curvilinear shell structures are commonly used in aeronautical, aerospace, automotive and other engineering applications. Thus, adaptive curvilinear composite shells with embedded piezoelectric devices are among the structural configurations of most practical interest, yet, they are also among the more challenging to study both analytically and experimentally. The present paper presents theoretical foundations and mechanics for the analysis of curvilinear piezoelectric laminates and shell structures.

Numerous theories and models have been proposed for the analysis of laminated composite beams and plates containing active and passive piezoelectric layers. Simplified approaches attempting to replicate the induced strains and electric fields generated by a piezoelectric layer under an external electric field have been proposed (see e.g. Lee and Moon (1989), Lee (1990), Lee and Moon (1990), Wang and Rogers (1991), Lazarus and Crawley (1989)). Variational methods and finite element models for piezoelectric solids have also been reported by Allik and Hughes (1970), Naillon et al. (1983), Tzou and Tseng (1990), and Ha et al. (1992). Layerwise theories were reported for infinite piezoelectric plates (Pauley (1974)) and for finite elastic laminated beams and plates with induced strain actuation (Robbins and Reddy (1991, 1993)). Coupled layerwise theories and finite elements for laminated composite beams and plates with piezoelectric actuators and sensors were also developed (Heyliger et al. (1994), Saravanos and Heyliger (1995), Saravanos and Heyliger (1996)) which consider the complete electromechanical response of smart piezoelectric plate structures under external mechanical or electrical loading. An exact piezoelasticity solution has been also reported by Heyliger and Saravanos (1995) for piezoelectric laminated plates.

Analytical formulations have been proposed for laminated piezoelectric shells. Dockmeci (1990) has reported theoretical work for the vibration of single-layered piezoelectric shells. Lammering (1991)

3

developed a Reissner-Middlin type shear deformable finite element for shells with surface bonded piezoelectric layers. Tzou and co-workers have presented approaches for the analysis of thin laminated shells based on Kirchoff-Love assumptions (Tzou and Garde (1989)), and theoretical formulations for shells which include Reissner-Middlin type of shear deformation theory and rotary inertia effects (Tzou and Zhong, 1993). Some of the previous approaches effectively utilize equivalent force/moment representations of the induced strain by attempting to replicate the electric fields in the piezoelectric layers and do not solve the coupled equations of piezoelectricity directly. Alternatively, (Tzou and Ye, 1996) proposed the analysis of piezoelectric shells as a layerwise assembly of curvilinear solid piezoelectric triangular elements, while Heyliger et al. (1996) developed discrete-layer mechanics and a finite element for laminated piezoelectric solids.

The work in this paper attempts to remedy some of the problems in previous works (uncoupled approaches, limitations in piezoelectric laminations, large problem sizes, and so forth) while maintaining some of their advantages (formulation in curvilinear coordinates, layerwise approach, computational efficiency). Consequently, this paper presents the theoretical foundations of a new coupled laminate theory and, more importantlly, the development and evaluation of a corresponding finite element which enables the formal anlaysis of piezoelectric composite shells. The mechanics are truly coupled, that is, they involve approximate through-the-thickness fields for both displacements and electric potential, and are formulated using the coupled equations of piezoelectricity in the curvilinear coordinates. Moreover, the proposed laminate shell theory utilizes different types of approximations for the displacement and electric potential, that is, first-order shear theory type of assumptions for the displacements and the so-called discrete-layer (or layerwise) approximation for the electric potential (Heyliger et. al. (1994); Saravanos and Heyliger (1995, 1996)). The combination of mixed through-the-thickness approximations for the displacement and electric potential is a unique feature of the mechanics (termed, thereafter, as "mixed-field laminate shell theory") which enables the analysis of thin and moderately thick piezoelectric shells of general laminations with reasonable computational efficiency, while maintaining sufficient detail in the approximation of the electrical fields. Structural mechanics are also formulated, based on the laminate shell theory for the numerical analysis of piezoelectric composite shells and an 8-node curvilinear shell element is developed.

Numerical results for laminated composite plates are compared with results from an exact solution. Additional cases investigate the quasi-static and free-vibration response of an adaptive composite ring with a piezoceramic layer, and the quasi-static response of a [0/90/45/-45], semi-circular composite shell with discrete cylindrical piezoelectric actuators and sensors.

2. Piezoelectric Laminated Shells

This section describes the analytical formulation for curvilinear laminates with embedded sensory and active piezoelectric layers. The curvilinear laminate configuration is shown schematically in Fig. 1. Each ply of the laminate remains parallel to a reference curvilinear surface A_o. An orthogonal curvilinear coordinate system $\bar{O}\xi\eta\zeta$ is defined, such that the axes ξ and η lie on the curvilinear reference surface A_o, while the axis ζ remains straight and perpendicular to the layers of the laminate. A global cartesian coordinate system $Oxyz$ is used to define A_o, hence, a point $r=(x,y,z)$ on the curvilinear laminate is,

$$r(\xi,\eta,\zeta)=r_o(\xi,\eta)+\zeta\hat{\zeta} \tag{1}$$

where, $r_o=(x_o,y_o,z_o)$ are the Cartesian coordinates of the reference surface A_o, and ζ overhat indicates the unit vector perpendicular to the reference surface.

Governing Material Equations

Each ply is assumed to consist of a linear piezoelectric material with properties defined on the orthogonal curvilinear system $\bar{O}\xi\eta\zeta$, and constitutive equations of the following form,

$$\begin{aligned}
S_i &= s_{ij}^E \sigma_j + d_{ik} E_k \\
D_l &= d_{lj} \sigma_j + \varepsilon_{lk}^\sigma E_k
\end{aligned} \tag{2}$$

or equivalently,

5

$$\sigma_i = C_{ij}^E S_j - e_{ik} E_k$$
$$D_l = e_{lj} S_j + \varepsilon_{lk}^S E_k$$

(3)

where: $i,j = 1,...,6$ and $k,l = 1,...,3$; σ_i and S_i are the mechanical stresses and engineering strains in vectorial notation; E_k is the electric field vector; D_l is the electric displacement vector; s_{ij} and C_{ij} are the elastic compliance and stiffness tensors; d_{ij} and e_{ij} are different forms of the piezoelectric tensor; and ε_{lk} is the electric permittivity tensor of the material. Superscripts E, σ, and S indicate constant electric field, stress and strain conditions, respectively. The axes 1, 2, and 3 of the material are parallel to the curvilinear axes ξ, η, and ζ, respectively. The materials are assumed to be monoclinic class 2 crystals with a diad axis parallel to the ζ axis. The assumed material class is general enough, such that eqs. (1) or (2) may encompass the behavior of off-axis homogenized piezoelectric plies, as well as, passive composite plies.

The tensorial strain S_{ij} and electric field components in a curvilinear coordinate system are related to the displacement and electric potential respectively as follows (Fung, 1965)

$$\bar{S}_{ij} = \frac{1}{2\sqrt{g_{ii}g_{jj}}}((\bar{u}_{i,j} + \bar{u}_{j,i}) - \bar{u}_k(\Gamma_{ij}^k + \Gamma_{ji}^k)) \qquad k=1,...,3$$

(4)

$$\bar{E}_i = -\frac{1}{\sqrt{g_{ii}}}\frac{\partial\phi}{\partial\bar{x}_i}$$

(5)

where: g_{ij} is the metric tensor and G_{ij}^k are the Christofel Symbols of the curvilinear system; the overbar was used to indicate tensorial components in the curvilinear system, and implied in the rest of the paper. For the case of the curvilinear system $\bar{O}\xi\eta\zeta$ defined in Fig. 1, the Euclidean metric tensor takes the form (Soedel, 1993),

$$g_{11} = (1+\zeta/R_1)^2 g_{11}^{o2}, \quad g_{22} = (1+\zeta/R_2)^2 g_{22}^{o2}, \quad g_{33} = 1$$

(6)

where R_i are the local radii of curvature, and g_{11}^o, g_{22}^o are the components of the metric tensor on the

surface A_o ($\zeta=0$) defined as

$$g_{11}^o = \sqrt{x_{o,\xi}^2 + y_{o,\xi}^2 + z_{o,\xi}^2} \ , \qquad g_{22}^o = \sqrt{x_{o,\eta}^2 + y_{o,\eta}^2 + z_{o,\eta}^2} \tag{7}$$

Consequently, after substituting in eq. (4) and with substantial derivations, the strain-displacement relationships become (see also, Soedel (1993)),

$$S_{11} = S_1 = \frac{1}{g_{11}^o(1+\zeta/R_1)}\left(u_{,\xi} + \frac{g_{11,\eta}^o}{g_{22}^o}v + \frac{g_{11}^o}{R_1}w\right)$$

$$S_{22} = S_2 = \frac{1}{g_{22}^o(1+\zeta/R_2)}\left(v_{,\eta} + \frac{g_{22,\xi}^o}{g_{11}^o}u + \frac{g_{22}^o}{R_2}w\right)$$

$$S_{12} = S_6 = \frac{1}{g_{11}^o(1+\zeta/R_1)}\left(v_{,\xi} - \frac{g_{11,\eta}^o}{g_{22}^o}u\right) + \frac{1}{g_{22}^o(1+\zeta/R_2)}\left(u_{,\eta} - \frac{g_{22,\xi}^o}{g_{11}^o}v\right) \tag{8}$$

$$S_{33} = S_3 = w_{,\zeta}$$

$$S_{23} = S_4 = v_{,\zeta} + \frac{1}{g_{22}^o(1+\zeta/R_2)}\left(w_{,\eta} - \frac{g_{22}^o}{R_2}v\right)$$

$$S_{13} = S_5 = u_{,\zeta} + \frac{1}{g_{11}^o(1+\zeta/R_1)}\left(w_{,\xi} - \frac{g_{11}^o}{R_1}u\right)$$

where u, v, w are displacements in the curvilinear system. Similarly, eq. (5) relates the electric field vector E_k to the electric potential ϕ as follows (similar to Tzou and Zhong (1993)),

$$E_1 = -\frac{1}{g_{11}^o(1+\zeta/R_1)}\,\phi_{,\xi}$$

$$E_2 = -\frac{1}{g_{22}^o(1+\zeta/R_2)}\,\phi_{,\eta} \tag{9}$$

$$E_3 = -\phi_{,\zeta}$$

Mixed Field Laminate Theory

A new laminate theory is proposed in this paper which assumes linear displacement fields through the thickness of the laminate for the displacements u, v (displacement along the x and h axes respectively) while the transverse displacement w remains constant through the thickness (Fig. 2). However, a layerwise electric potential field is assumed through the laminate, consisting of N discrete continuous

segments (Fig. 2). Previous work by Saravanos and Heyliger on layerwise theories for piezoelectric plates has demonstrated the advantages and necessity of layerwise approaches in capturing the complicated electric fields and interactions which are present in piezoelectric actuators and sensors. Consequently, by mixing a layerwise electric potential field with first-order shear theory assumptions for the displacements, a new piezoelectric shell laminate theory is postulated (termed accordingly as "mixed-field laminate theory") which can: (1) capture the electric heterogeneity through-the-thickness induced by the embedded piezoelectric sensors & actuators, and (2) model thin and/or moderately thick piezoelectric shell laminates with minimal computational cost.

The laminate is subdivided in N-1 piezoelectric sublaminates (or discrete-layers), and the subdivision can be arbitrarily controlled according to the configuration of the piezoelectric layers and/or the required detail of approximation. A continuous electric potential is assumed in each sublaminate, such that a C_o continuous variation results through the thickness of the laminate (see Fig. 2). The displacements and electric potential of the mixed-field theory take the following form,

$$u(\xi,\eta,\zeta,t) = u^o(\xi,\eta,t) + \zeta\beta_\xi(\xi,\eta,t)$$
$$v(\xi,\eta,\zeta,t) = v^o(\xi,\eta,t) + \zeta\beta_\eta(\xi,\eta,t)$$
$$w(\xi,\eta,\zeta,t) = w^o(\xi,\eta,t)$$
$$\phi(\xi,\eta,\zeta,t) = \sum_{j=1}^{N} \phi^j(\xi,\eta,t)\Psi^j(\zeta)$$

(10)

where u^o, v^o, w^o are displacements along the ξ, η and ζ axes, respectively, on the reference surface A_o; superscript j indicates the points ζ^j at the beginning and end of each discrete layer; ϕ^j is the electric potential at each point ζ^j (see Fig. 2); $\Psi^j(z)$ are interpolation functions; and β_ξ, β_η are the rotation angles defined as,

$$\beta_\xi = -\frac{w^o_{,\xi}}{g^o_{11}} + \frac{u^o}{R_1}$$

$$\beta_\eta = -\frac{w^o_{,\eta}}{g^o_{22}} + \frac{v^o}{R_2}$$

(11)

Two unique advantages of the laminate theory are obvious: (1) the complete electromechanical state

8

of the smart laminate is represented; and (2) the formulation entails the inherent option to select the detail of approximation of the electric field. Linear interpolation functions $\Psi(z)$ were considered in this paper.

The Love's assumption is further implemented, that is, the local radii of the shell are substantially higher than the thickness ($h/R_i << 1$), yielding ($1+ \zeta/R_i \approx 1$). The Love's assumption is appropriate for shallow shells, yet, additional work will be presented in the near future for deep shells with the Love's assumption removed. Now, in the context of eqs. (10), the engineering strains become,

$$S_i(\xi,\eta,\zeta,t) = S_i^o(\xi,\eta,t) + \zeta k_i(\xi,\eta,t) \qquad i=1,2,6$$
$$S_3(\xi,\eta,\zeta,t) = 0 \tag{12}$$
$$S_i(\xi,\eta,\zeta,t) = S_i^o(\xi,\eta,t) \qquad i=4,5$$

where S^o and k are the strain and curvatures at the reference surface, defined as follows:

$$S_1^o = \frac{1}{g_{11}^o}(u_{,\xi}^o + \frac{g_{11,\eta}^o}{g_{22}^o}v^o) + \frac{w^o}{R_1}, \qquad S_2^o = \frac{1}{g_{22}^o}(v_{,\eta}^o + \frac{g_{22,\xi}^o}{g_{11}^o}u^o) + \frac{w^o}{R_2}$$

$$S_6^o = \frac{1}{g_{11}^o}(v_{,\xi}^o - \frac{g_{11,\eta}^o}{g_{22}^o}u^o) + \frac{1}{g_{22}^o}(u_{,\eta}^o - \frac{g_{22,\xi}^o}{g_{11}^o}v^o) \tag{13}$$

$$S_4^o = \beta_\eta + \frac{w_{,\eta}^o}{g_{22}^o} - \frac{v^o}{R_2}, \qquad S_5^o = \beta_\xi + \frac{w_{,\xi}^o}{g_{11}^o} - \frac{u^o}{R_1}$$

$$k_1 = \frac{1}{g_{11}^o}(\beta_{\xi,\xi} + \frac{g_{11,\eta}^o}{g_{22}^o}\beta_\eta), \qquad k_2 = \frac{1}{g_{22}^o}(\beta_{\eta,\eta} + \frac{g_{22,\xi}^o}{g_{11}^o}\beta_\xi)$$

$$k_6 = \frac{1}{g_{11}^o}(\beta_{\eta,\xi} - \frac{g_{11,\eta}^o}{g_{22}^o}\beta_\xi) + \frac{1}{g_{22}^o}(\beta_{\xi,\eta} - \frac{g_{22,\xi}^o}{g_{11}^o}\beta_\eta) \tag{14}$$

The electric field vector also becomes,

$$E_i(\xi,\eta,\zeta,t) - \sum_{j=1}^{N} E_i^j(\xi,\eta,t)\Psi^j(\zeta) \qquad i-1,2$$

$$E_3(\xi,\eta,\zeta,t) - \sum_{j=1}^{N} E_3^j(\xi,\eta,t)\Psi_{,\zeta}^j(\zeta)$$

(15)

where $\{E^j\}$ is the generalized electric field vector defined as:

$$E_1^j - \frac{\Phi_{,\xi}^j}{\overset{o}{g}_{11}} \qquad E_2^j - \frac{\Phi_{,\eta}^j}{\overset{o}{g}_{22}} \qquad E_3^j - \Phi^j$$

(16)

Equations of Motion

The variational form of the equations of motion in the orthogonal curvilinear system is,

$$\int_V \{ -(\delta H(S,E)-\delta T \}|J|d\xi\,d\eta\,d\zeta + \oint_\Gamma (\delta u_i^T \bar\tau_i - \delta\phi\bar D)d\Gamma - 0$$

(17)

where δH is the variation of the electric enthalphy and δT the variation of the kinetic energy, defined as,

$$\delta H - \delta S_i \sigma_i - \delta E_k D_k - \delta S_i C_{ij} S_j - \delta E_k e_{kj} S_j - \delta S_i e_{il} E_l - \delta E_k \varepsilon_{kl} E_l$$
$$\delta T - -\delta u_i \rho_i \ddot u_i$$

(18)

τ and D overbar are respectively the surface tractions and electric displacement on the boundary surface Γ,

$$\bar\tau_i - \sigma_{ij}\hat n_j \qquad \bar D - D_j\hat n_j \qquad i,j-1,...,3$$

(19)

[J] is the jacobian matrix of the transformation between the global Cartesian and curvilinear system. For the curvilinear system $\bar O\xi\eta\zeta$ the determinant of the Jacobian takes the form:

$$|J| - |\frac{\partial(x,y,z)}{\partial(\xi,\eta,\zeta)}| - \sqrt{g_{11}g_{22}} - \overset{o}{g}_{11}\overset{o}{g}_{22}(1+\zeta/R_1)(1+\zeta/R_2) \approx \overset{o}{g}_{11}\overset{o}{g}_{22}$$

(20)

It is now possible to rearrange the variational statement and separate the through-the-thickness

integration, as follows:

$$\int_{A_\bullet}\{\int_0^h -(\delta H(S,E)-\delta T)\overset{o}{g}_{11}\overset{o}{g}_{22}d\zeta\}\,d\xi\,d\eta \;+\; \oint_\Gamma (\delta u_i^T \overset{\sim}{\tau}_i + \delta\phi\bar{D})d\Gamma = 0 \tag{21}$$

The electric enthalpy and kinetic energy of the laminate may now be defined as,

$$<\delta H_L,\delta T_L> = \int_0^h <\delta H,\delta T>\overset{o}{g}_{11}\overset{o}{g}_{22}\,d\zeta \tag{22}$$

where h is the laminate thickness. By combining eqs. (18,22) and integrating through-the-thickness, the variation of the electric enthalpy of the piezoelectric laminate is obtained as a quadratic expression of the generalized strain/electric field and the generalized laminate stiffness, piezoelectric and dielectric permittivity matrices,

$$\delta H_L = \delta \overset{o}{S}_i A_{ij}\overset{o}{S}_j + \delta \overset{o}{S}_i B_{ij} k_j + \delta k_i B_{ji}\overset{o}{S}_i + \delta k_i D_{ij} k_j -$$
$$-\sum_{m-1}^{N}(\delta\overset{o}{S}_i \bar{E}_{ik}^m E_k^m + \delta E_k^m \bar{E}_{ik}^m \overset{o}{S}_i + \delta k_j \hat{E}_j^m E_3^m + \delta E_3^m \hat{E}_j^m k_j) -\sum_{i-1}^{N}\sum_{i-1}^{N}\delta E_k^m G_{kl}^{mn} E_l^m \tag{23}$$

In the above equation, [A], [B], and [D] are the stiffness matrices of the curvilinear laminate,

$$< A_{ij},\, B_{ij},\, D_{ij} > = \overset{o}{g}_{11}\overset{o}{g}_{22}\sum_{L-1}^{L}\int_{\zeta_l}^{\zeta_{l+1}}C_{ij}<1,\zeta,\zeta^2>d\zeta, \qquad i,j-1,2,6$$
$$A_{ij} = \overset{o}{g}_{11}\overset{o}{g}_{22}\sum_{L-1}^{L}\int_{\zeta_l}^{\zeta_{l+1}}C_{ij}d\zeta, \qquad i,j-4,5, \tag{24}$$

[E^m] overbar and overhat are the piezoelectric laminate matrices,

$$< \bar{E}_{ij}^m,\hat{E}_{ij}^m > = \overset{o}{g}_{11}\overset{o}{g}_{22}\sum_{L-1}^{L}\int_{\zeta_l}^{\zeta_{l+1}}e_{ij}\Psi_{,\zeta}^m(\zeta)<1,\zeta>d\zeta, \qquad i-3,\; j-1,2,6$$
$$\bar{E}_{ij}^m = \overset{o}{g}_{11}\overset{o}{g}_{22}\sum_{L-1}^{L}\int_{\zeta_l}^{\zeta_{l+1}}e_{ij}\Psi^m(\zeta)d\zeta, \qquad i-1,2,\; j-4,5 \tag{25}$$

and [G^{mn}] are the laminate matrices of electric permittivity,

11

$$G_{tt}^{mn} = \overset{o}{g}_{11}\overset{o}{g}_{22} \sum_{L=1}^{L} \int_{\zeta_l}^{\zeta_{l+1}} e_{tt}\ \Psi^m(\zeta)\Psi^n(\zeta)d\zeta$$

$$G_{33}^{mn} = \overset{o}{g}_{11}\overset{o}{g}_{22} \sum_{L=1}^{L} \int_{\zeta_l}^{\zeta_{l+1}} e_{33}\Psi_{,\zeta}^m(\zeta)\Psi_{,\zeta}^n(\zeta)d\zeta \tag{26}$$

where L is the number of plies in the laminate. All remaining matrix terms not shown above are zero.

Combining equations (18, 22) and integrating through-the-thickness, the kinetic energy of the laminate takes the form,

$$\delta T_L = \delta u_i^o \rho_i^A \dot{u}_i^o + \delta u_j^o \rho_j^B \dot{\beta}_j + \delta\beta_j \rho_j^B \dot{u}_j + \delta\beta_j \rho_j^D \dot{\beta}_j, \qquad i=1,...,3,\ j=1,2 \tag{27}$$

where $u_i^o = \{u^o, v^o, w^o\}$ and $\beta_i = \{\beta_\xi, \beta_\eta\}$; ρ^A, ρ^B, ρ^D are the generalized densities, expressing the mass, mass coupling and rotational inertia per unit area, respectively, of the laminate,

$$<\rho^A, \rho^B, \rho^D> = \overset{o}{g}_{11}\overset{o}{g}_{22} \sum_{L=1}^{L} \int_{\zeta_l}^{\zeta_{l+1}} \rho_l <1, \zeta, \zeta^2> d\zeta \tag{28}$$

3. Piezoelectric Shell Structures

The formulation of the governing equations in the orthogonal curvilinear system and the attained separation of the through-the-thickness integration in the equation of motion (21) enables the development of structural solutions by using approximations of the generalized electromechanical state (displacements, rotation angles and electric potential) on the reference surface A_o, of the following type,

$$u_j^o(\xi,\eta,t) = \sum_{i=1}^{M} u_j^{\alpha}(t)\, N^i(\xi,\eta), \qquad j=1,...,3$$

$$\beta_j(\xi,\eta,t) = \sum_{i=1}^{M} \beta_j^i(t)\, N^i(\xi,\eta), \qquad j=1,2 \tag{29}$$

$$\phi^m(\xi,\eta,t) = \sum_{i=1}^{M} \phi^{mi}(t)\, N^i(\xi,\eta), \qquad m=1,...,N$$

where superscript i indicates the reference surface displacement, rotation angle and generalized

12

electric potential components corresponding to the i-th in-plane interpolation function $N^i(x,y)$. This formulation forms the basis for an number of approximate solutions. Combining eqs. (13, 14, 16, 29), the generalized laminate strains and electric field at a point (ξ,η) of the reference surface A_o take the form:

$$
\begin{Bmatrix} S_1^o \\ S_2^o \\ S_4^o \\ S_5^o \\ S_6^o \end{Bmatrix} =
\begin{bmatrix}
N_{,\xi}^i/g_{11}^o & N^i g_{11,\eta}^o/g_{11}^o g_{22}^o & N^i/R_1 & 0 & 0 \\
N^i g_{22,\xi}^o/g_{11}^o g_{22}^o & N_{,\eta}^i/g_{22}^o & N^i/R_2 & 0 & 0 \\
0 & -N^i/R_2 & N_{,\eta}^i/g_{22}^o & 0 & N^i \\
-N^i/R_1 & 0 & N_{,\xi}^i/g_{11}^o & N^i & 0 \\
-N^i g_{11,\eta}^o/g_{11}^o g_{22}^o + N_{,\eta}^i/g_{22}^o & N_{,\xi}^i/g_{11}^o - N^i g_{22,\xi}^o/g_{11}^o g_{22}^o & 0 & 0 & 0
\end{bmatrix}
\begin{Bmatrix} u^{\alpha i} \\ v^{\alpha i} \\ w^{\alpha i} \\ \beta_\xi^i \\ \beta_\eta^i \end{Bmatrix}
\tag{30}
$$

$$
\begin{Bmatrix} k_1 \\ k_2 \\ k_6 \end{Bmatrix} =
\begin{bmatrix}
N_{,\xi}^i/g_{11}^o & N^i g_{11,\eta}^o/g_{11}^o g_{22}^o \\
N^i g_{22,\xi}^o/g_{11}^o g_{22}^o & N_{,\eta}^i/g_{22}^o \\
-N^i g_{11,\eta}^o/g_{11}^o g_{22}^o + N_{,\eta}^i/g_{22}^o & N_{,\xi}^i/g_{11}^o - N^i g_{22,\xi}^o/g_{11}^o g_{22}^o
\end{bmatrix}
\begin{Bmatrix} \beta_\xi^i \\ \beta_\eta^i \end{Bmatrix}
\tag{31}
$$

$$
\begin{Bmatrix} E_1^m \\ E_2^m \\ E_3^m \end{Bmatrix} =
\begin{bmatrix}
-N_{,\xi}^i/g_{11}^o \\
-N_{,\eta}^i/g_{22}^o \\
-N^i
\end{bmatrix}
\{\phi^{mi}\} , \qquad i = 1,...,M
\tag{32}
$$

Finite Element Formulation

For structural problems with general boundary, geometry and material configurations, local interpolation functions may be used in eqs. (29) to develop finite-element based solutions. Substituting these approximations into the generalized equation of motion (21) and collecting the coefficients, as mandated by eqs. (23, 27), the governing dynamic equations of the structure are expressed in a discrete matrix form as,

$$
\begin{bmatrix} [M_{uu}] & 0 \\ 0 & 0 \end{bmatrix}
\begin{Bmatrix} \{\ddot{U}\} \\ \{\ddot{\phi}\} \end{Bmatrix} +
\begin{bmatrix} [K_{uu}] & [K_{u\phi}] \\ [K_{\phi u}] & [K_{\phi\phi}] \end{bmatrix}
\begin{Bmatrix} \{U\} \\ \{\phi\} \end{Bmatrix} =
\begin{Bmatrix} \{F(t)\} \\ \{Q(t)\} \end{Bmatrix}
\tag{33}
$$

The above submatrices K_{uu}, $K_{u\phi}$ and $K_{\phi\phi}$ are the elastic, piezoelectric and permitivity matrices and M_{uu} is the mass matrix. They are calculated from the generalized laminate matrices defined in eqs. (24-26) as determined by the variational statement. At each finite element they take the form:

$$[K_{uu}]^{ij} = \int_{A_{oe}} [R^{\alpha i}]^T \begin{bmatrix} [A] & [B] \\ [B] & [D] \end{bmatrix} [R^{\alpha j}] \, d\xi \, d\eta$$

$$[K_{u\phi}^{m}]^{ij} = \int_{A_{oe}} [R^{\alpha i}]^T \begin{bmatrix} [\bar{E}^{m}]^T \\ [\hat{E}^{m}]^T \end{bmatrix} [R^{mj}] \, d\xi \, d\eta \qquad (34)$$

$$[K_{\phi\phi}^{mn}]^{ij} = \int_{A_{oe}} [R^{mi}]^T [G^{mn}] R^{nj} \, d\xi \, d\eta$$

$$[M_{uu}]^{ij} = \int_{A_{oe}} [N^{\alpha i}]^T \begin{bmatrix} [diag(\rho^A)] & [diag(\rho^B)] \\ [diag(\rho^B)] & [diag(\rho^D)] \end{bmatrix} [N^{\alpha j}] \, d\xi \, d\eta$$

where: $R^{\alpha i}$ and R^{mi} are the strain and electric field interpolation matrices defined by eqs. (30-31) and (32), respectively; $N^{\alpha i}$ are the displacement interpolation functions defined by eq. (29).

Based on the above formulation, an 8-node (M=8) finite element was developed with bi-quadratic shape functions of the serendipity family. The same interpolation functions are used to define the reference surface with respect to the coordinates of each node at the Cartesian system Oxyz

$$(x^o, y^o, z^o) = \sum_{i=1}^{M} N^i(\xi, \eta) \, (x^{\alpha i}, y^{\alpha i}, z^{\alpha i}) \qquad (35)$$

The radii R_1, R_2 and the coefficients g^o_{11}, g^o_{22} (eq. 7) of the reference surface are calculated in each element based on the previous parametric surface representation.

Assuming that both sensory and active piezoelectric layers are embedded into the structure, the electric potential vector is subdivided in a free or sensory component ϕ^F representing the voltage output at the sensors, and a forced or active component ϕ^A representing the voltage imposed on the active piezoelectric layers, such that $\{\phi\} = \{ \phi^F ; \phi^A \}$. Separating the active and sensory potential components in eq. (33), the equations take the following form

14

$$\begin{bmatrix} [M_{uu}] & 0 \\ 0 & 0 \end{bmatrix} \begin{Bmatrix} \{\ddot{u}\} \\ \{\ddot{\phi}^F\} \end{Bmatrix} + \begin{bmatrix} [K_{uu}] & [K_{u\phi}^{FF}] \\ [K_{\phi u}^{FF}] & [K_{\phi\phi}^{FF}] \end{bmatrix} \begin{Bmatrix} \{u\} \\ \{\phi^F\} \end{Bmatrix} = \begin{Bmatrix} \{F(t)\}-[K_{u\phi}^{FA}]\{\phi^A\} \\ \{Q^F(t)\}-[K_{\phi\phi}^{FA}]\{\phi^A\} \end{Bmatrix} \qquad (36)$$

where superscripts F and A indicate the partitioned submatrices in accordance with the selected sensory and active configuration, respectively. The left-hand side includes the unknown electromechanical response of the structure $\{u, \phi^F\}$, that is, the resultant displacements and voltage at the sensors. The right-hand includes the excitation of the structure in terms of mechanical loads and applied voltages on the actuators. The electric charge at the sensors $Q^F(t)$ remains constant with time (practically open-circuit conditions) and is assumed equal to zero.

Among the obvious advantages is the capability of the mechanics to model the response of the piezoelectric structure either: in "active" mode, that is, with specified voltages $\Delta\phi^A$ applied across the piezoelectric layers to induce a desirable deflection/strain state; or in "sensory" mode where displacements or mechanical loads are applied to the structure and the resultant voltage or charge is monitored; or in combined "active/sensory" mode. The above dynamic system may be solved to obtain, either the modal characteristics (free-vibration), or the forced frequency response, or the transient response of the piezoelectric shell.

4. Evaluations and Discussion

Applications and evaluations of the developed mechanics on various piezoelectric structures are presented in this section. As in previous publications, the standard laminate notation is expanded such that piezoelectric layers are indicated with the letter p. Results are presented for simply supported [p/0/90/0/p] cross-ply Graphite/Epoxy composite plates with attached piezoceramic (PZT-4) layers. Results are also presented for two cylindrical shell structures: (1) a closed cylindrical titanium shell [Ti/p] with a continuous piezoceramic (PZT-4) layer on the outer surface; and (2) a cantilever semi-circular laminated [0/90/45/-45], Graphite/Epoxy shell with distributed cylindrical piezoceramic (PZT-4) patches on the inner and outer surface. The

properties of the materials are provided in Table 1.

[p/0/90/0/p] Hybrid Plate

Results are presented for the free-vibration response of simply supported [p/0/90/0/p] cross-ply Graphite/Epoxy composite plates with surface attached piezoceramic (PZT-4) layers. The electric potential on the outer (free) surface of the piezoelectric layers was always forced to remain zero. The electric potential in the inner surface may be either free or forced to remain zero, resulting in two different electric boundary conditions, termed as open- and closed-circuit conditions respectively. The thickness of each composite ply and piezoelectric layer are 0.267h and 0.1h respectively, where h is the plate thickness. The composite plies and piezoelectric material were assumed to have equal mass density in this case. The response of these plates has been previously studied via exact solutions (Heyliger et. al. 1995) and discrete-layer mechanics (Saravanos and Heyliger, 1996), hence, their analysis provides excellent assessments of the accuracy and range of capabilities of the present mechanics .

Table 2 shows predictions of the fundamental natural frequency for a moderately thin plate (a/h=50) and a thick plate (a/h=4) with either open or closed-circuit conditions imposed on the piezoelectric layers. The case of interest here is the moderately thin plate because the mechanics are developed for thin and moderatelly thick shells; whereas, the thick plate example is an extreme case presented to quantify any limitations of the present approach. In the case of the thin plate, the predicted natural frequencies converge, either as the in-plane mesh density is increasing (M) or the number of discrete layers for the electric potential through-the-thickness (N). More importantly, the predicted natural frequency agrees well with the exact piezoelasticity solution. As expected, lower frequency values were predicted for closed (C), than with open (O) circuit conditions. Figs. 3a-b shows the predicted modal displacements and electric potential fields through-the-thickness of the thin plate, and as seen, excellent agreement was obtained between the present approach and the exact solution. Although the present method is not indended for thick shells, results for the case of a thick plate are also presented in Table 2 and Fig. 4. The predicted frequency values in

16

Table 2 overestimate the exact solution results by 12.7% and 21.5% for (O) and (C) conditions, respectively, as the laminate theory does not capture the layerwise variations in the displacement fields (Fig. 4a-b). However, Fig. 4c shows that the present method did capture the layerwise variations of the modal electric potential and yielded excellent agreement with the exact solution.

Closed Cylindrical Shell

Results for the quasi-static and free-vibration response of an active/sensory cylindrical ring are presented in this section. The ring consisted of one 3 mm thick Titanium layer and one continuous piezoceramic layer of PZT-4 (1 mm thick) attached on the outer surface. The inner radius was 289 mm, and the width was 348 mm. Fig. 5 shows one quarter of the ring, the laminate configuration and the curvilinear coordinate system which was used. Symmetry conditions were applied at two planes of symmetry (at $\theta = 0$ and 90°) in the circumferencial direction (ξ) , and at the plane of symmetry in the axial direction (η) in order to reduce the size of the model. Two discrete layers (N=3) were used for the electric potential field through-the-thickness (ζ), one for the piezoelectric and one for the titanium layer. The electric potential in the inner surface of the piezoelectric layer was always equal to 0 Volts. Two types of loading conditions were examined: (1) application of a sinusoidal electric potential on the outer surface of the piezoelectric layer; (2) application of mechanical load with free electric potential on the outer piezoelectric surface. Apparently, the previous two loading conditions were selected to investigate the active and sensory response, respectively, of the cylindrical shell.

Active Ring. The radial displacements at $\theta = 0$ and 90° at the center of the ring (along the η axis), induced by a sinusoidal electric potential (100cos2θ Volts) applied on the outer surface of the piezoelectric actuator, are shown in Table 3 for various mesh densities. The first five natural frequencies of the active ring are also shown in Table 3 which correspond to closed-circuit electric conditions. The induced displacements and the natural frequencies seem to converge well as the mesh density increases. There is also very good agreement between the present predictions and numerical results obtained with a recently developed layerwise finite-element for

17

laminated piezoelectric solids (Heyliger et. al, 1996), which validates the accuracy of the present method. Fig. 6 shows the induced active radial deflections along the circumferencial direction at the center and the free edge of the active ring. The applied sinusoidal electric potential produces an almost pure ovalization of the active shell. Considering that the applied voltage in this example was approximately 4 times lower that the maximum allowed voltage on the actuator, the maximum active deflection which may be effectively induced is not insignificant. Such ovalization capabilities may be important to many aeronautical applications.

Sensory Ring. This example examines the behavior of the piezoelectric layers as a distributed sensor. The electric potential on the outer surface of the piezoelectric layer remains free, while a radial line load $F_\zeta = 656$ N/m was applied at $\theta = 90°$. As in the previous case, induced deflections, sensory potential and natural frequencies of the sensory ring are shown in Table 4, together with convergence studies and correlations with other published results. Again the convergence of the present study is excellent, with the sensory electric potential requiring the higher mesh density. The agreement between the present method and layerwise piezoelectric solid mechanics (Heyliger et al., 1996) ranges from excellent (natural frequencies) to fair (displacements). The variations of the radial deflection and corresponding sensory electric potential in the hoop direction are shown in Fig. 7. The application of the line load also results in the ovalization of the ring, and the sensory potential has a nearly sinusoidal form. The results in Fig. 7 demonstrate the usefulness of the present mechanics in predicting the not so apparent sensory voltage patterns in distributed piezoelectric sensors which correspond to various deformed shapes of a smart shell structure. The usefulness of these predictions in estimating the minimum number and location of discrete piezoelectric patches is also apparent. Yet, as shown in the next case, the method has the capability to explicitly analyze the response of active/sensory composite shells with discrete piezoelectric actuators and sensors.

[0/90/+45/-45]$_s$ Cantilever Semi-Circular Shell

The response of a semi-circular cantilever [0/90/+45/-45]$_s$ Graphite/Epoxy smart shell shown in

18

Fig. 8 was also analyzed. Four curved piezoceramic (PZT-4) patches are attached on each side of the composite shell, covering 80% of the free area. The mid-surface radius is 291 mm and the width of the shell (L_η) is 152.4 mm. The thickness of each composite ply is 0.12 mm, while the thickness of each piezoelectric patch is 0.24 mm. The curvilinear coordinate system and the finite element discretization are also shown in Fig. 8b. Three discrete layers (N=4) were used for the electric potential field through-the-thickness (ζ), one for each piezoelectric layer and one for the composite laminate. In all cases, the electric potential at the bonded surface of the piezoelectric patches was forced to remain zero. The specification of the other two generalized electric potential values can result in various active and/or sensory configurations of the smart shell. Two such active and sensory configurations were analyzed.

Active Case. The induced active deflections in the radial (w^o) and hoop direction (u^o) are shown in Fig. 9. All piezoceramic patches were configured as actuators, with 100 Volts applied on their free surfaces, thus resulting in electric fields of opposite polarities at the piezoceramics of the inner and outer surface. For comparison purposes, the radial and circumferencial deflections of the shell with continuous piezoceramic layers of same thickness are also shown in Fig. 9. Although, the calculated deflections with either the discrete or the continuous piezoceramic actuators seem to be in good agreement, the effect of discrete actuators on the deflected shape of the shell is obvious. These effects can be attributed to the non-uniform actuation and the non-uniform laminate stiffness resulting from the piezoelectric patches. It is important to point out, however, the relatively high radial and hoop deflections at the free-end (approximately 5 mm) obtained in this case. It highlights the possibility to achieve substantialy large, yet, accurate and rapid free-end positioning with such active cantilever rings.

Sensory Case. The response of the cantilever shell with all piezoelectric patches configured as sensors (free electric potential) was also modelled. The more realistic case of continuous electrodes on the free surface of each sensor was also modeled. A continuous surface electrode forces a uniform electric potential over the surface, which was represented with equality constraints on the electric potential. A line load in the hoop direction F_ξ = 656 N/mm was applied

at the free end. The resultant displacements and corresponding voltages at each sensor are shown in Figs. 10a-b, respectively. The predicted response in the case of continuous piezoelectric layers is also shown. The presence of discrete piezoelectric sensors has a definite effect on the deflected shape. It is believed that the effects on the deflected shapes have resulted in the more dramatic differences between the voltage of discrete vs. continuous sensors. Fig. 10 also illustrates that the response of discrete sensors may be only roughly approximated with the consideration of a continuous layer. Hence, many proposed methods which attempt to replicate discrete sensors with segments of a continuous piezoelectric layer may lead to considerable error.

5. Summary

Mechanics for the analysis of laminated composite shells with piezoelectric actuators and sensors were presented. The mechanics were based on a new mixed-field theory for curvilinear laminates which combines single-layer assumptions for the displacements with a layerwise representation of the electric potential. The resulting governing coupled equations for piezoelectric shell laminates and structures were developed in curvilinear coordinates. Based on them, finite-element based analysis procedures for piezoelectric composite shell structures were described, and an 8-node shell finite-element was formulated for the static and dynamic analysis of composite shells containing piezoelectric actuators and sensors. The described mechanics, the finite element and the computational procedure were encoded in prototype software.

Excellent correlations with previously reported results for thin piezoelectric plates were obtained. Additional evaluations and comparisons were reported for the active and sensory response of a titanium cylindrical ring with a continuous piezoceramic actuator or sensor, and the capability to actively ovalize closed cylindrical shells was illustrated. Finally, the response of cantilever semi-circular laminated Graphite/Epoxy shells with discrete piezoelectric patches was also analyzed.

Acknowledgement

References

Allik H. and Hughes T. J. R. (1970). Finite Element for Piezoelectric Vibration. *International J. for Numerical Methods in Engineering* **2**, 151-157.

Crawley E. F. and Lazarus K. B. (1989). Induced Strain Actuation of Composite Plates. *AIAA Paper 89-1326-CP, 30th AIAA Structural Dynamics and Materials Conference*, Mobile, Alabama.

Docmeci C. M. (1990). Shell Theory for Vibrations in Piezoceramics under a Bias. *IEEE Transcactions on Ultrasonics, Ferroelectrics, and Frequency Control*, 37:5, 369-385.

Fung Y. C. (1965). *Foundations of Solid Mechanics*, Prentice-Hall, Inc. Englewood Cliffs, New Jersey.

Ha S. K., Keilers C. and Chang F. K. (1992). Finite Element Analysis of Composite Structures Containing Distributed Piezoceramic Sensors and Actuators. *AIAA J.* **30**:3, 772-780.

Heyliger P. R., Ramirez G. and Saravanos D. A. (1994). Coupled Discrete-Layer Finite Elements for Laminated Piezoelectric Plates. *Communications in Numerical Methods in Engineering* **10**, 971-981.

Heyliger P. R. and Saravanos D. A. (1995). Exact Free-Vibration Analysis of Laminated Plates with Embedded Piezoelectric Layers. *J. of Acoustical Society of America* **98**:3.

Heyliger P. R., Pei K. C. and Saravanos D. A. (in review). Layerwise Mechanics and Finite Element

Model for Laminated Piezoelectric Shells. *AIAA J.*

Lammering R. (1991). The Application of a Finite Shell Element for Composites Containing Piezoelectric Polymers in Vibration Control. *Computers and Structures* **41**, 1101-1109.

Lee C. K. and Moon F. C. (1989). "Laminated Piezopolymer Plates for Torsion and Bending Sensors and Actuators. *J. of the Acoustical Society of America* **85**, 2432-2439.

Lee C. K. (1990). Theory of Laminated Piezoelectric Plates for the Design of Distributed Sensors/Actuators. Part I: Governing Equations and Reciprocal Relationships. *J. of the Acoustical Society of America* **87**, 1144-1158.

Lee C. K. and Moon F. C. (1990). Modal Sensors/Actuators. *J. of Applied Mechanics* **57**, 434-441.

Naillon M., Coursant R. H. and Besnier F. (1983). Analysis of Piezoelectric Structures by a Finite Element Method. *Acta Electronica* **25**, 341-362.

Pauley K. P. (1974). Analysis of Plane Waves in Infinite, Laminated, Piezoelectric Plates, *Ph.D. Dissertation*, University of California at Los Angeles.

Robbins D. H. and Reddy J. N. (1991). Analysis of Piezoelectrically Actuated Beams Using a Layer-Wise Displacement Theory. *Computers and Structures* **41**, 265-279.

Robbins D. H. and Reddy J. N. (1993). Modelling of Thick Composites Using a Layerwise Laminate Theory. *International J. for Numerical Methods in Engineering* **36**, 655-677.

Saravanos D.A. and Heyliger P. R. (1995). Coupled Layerwise Analysis of Composite Beams with Embedded Piezoelectric Sensors and Actuators. *J. of Intelligent Material Systems and Structures* **6**:3, pp. 350-363.

Saravanos D. A., Heyliger P. R., and Hopkins D. A. (in press). Layerwise Mechanics and Finite Element for the Dynamic Analysis of Piezoelectric Composite Plates. Int. J. of Solids and Structures.

Soedel W. (1993). Deep Shell Equations. *Vibrations of Shells and Plates*, Marcel Dekker, Inc. New York, NY.

Tiersten H. F. (1969). *Linear Piezoelectric Plate Vibrations*, Plenum Press, New York.

Tzou H. S. and Garde M. (1989). Theoretical Analysis of a Multi-Layered Thin Shell Coupled with Piezoelectric Shell Actuators for Distributed Vibration Controls. J. of Sound and Vibration. 132:3, 433-450.

Tzou H. S. and Tseng C. I. (1990). Distributed Piezoelectric Sensor/Actuator Design for Dynamic Measurement/Control of Distributed Parametric Systems: A Piezoelectric Finite Element Approach. *J. of Sound and Vibration* **138**, 17-34.

Tzou H. S. and Zhong (1993). Electromechanics and Vibrations of Piezoelectric Shell Distributed Systems. J. of Dynamic Systems, Measurement and Control. 115, 506:517.

Tzou H. S. and Ye R. (1996). Analysis of Piezoelastic Structures with Laminated Piezoelectric Triangle Shell Elements. 34:8, (in press).

Wang B. T. and Rogers C. A. (1991). Laminate Plate Theory for Spatially Distributed Induced Strain Actuators. *J. of Composite Materials* **25**, 433-452.

Table 1 Mechanical Properties
(ε_o=8.85 10^{-12} farad/m, electric permittivity of air)

Property	Titanium	Gr/Epoxy	PZT-4
Elastic Properties:			
E_{11} (GPa)	114	132.4	81.3
E_{22} (GPa)	114	10.8	81.3
E_{33} (GPa)	114	10.8	64.5
G_{23} (GPa)	43.8	3.6	25.6
G_{13} (GPa)	43.8	5.6	25.6
G_{12} (GPa)	43.8	5.6	30.6
ν_{12}	0.3	0.24	0.33
ν_{13}	0.3	0.24	0.43
ν_{23}	0.3	0.49	0.43
Piezoelectric coefficients (10^{-12} m/V):			
d_{31}	0	0	-122
d_{32}	0	0	-122.
d_{24}	0	0	495.
d_{15}	0	0	495.
Electric Permittivity:			
$\varepsilon_{11}/\varepsilon_o$	1475.	3.5	1475.
$\varepsilon_{22}/\varepsilon_o$	1475.	3.0	1475.
$\varepsilon_{33}/\varepsilon_o$	1475.	3.0	1300.
Mass Density ρ(kg/m^3)	2768.	1578.	7600.

Table 2. Predicted Natural Frequencies of [p/0/90/0/p] square simply supported plate.
(C)- closed circuit; (O)- open circuit

Mesh Density	Discrete Layers (N-1)	Fundamental Frequency, $f_1 a^2/h \, \rho^{1/2}$ 10^3 Hz $(kg/m)^{1/2}$			
		$a/h=50$ (C)	$a/h=50$ (O)	$a/h=4$ (C)	$a/h=4$ (O)
4x4	3	236.390	258.673	255.052	176.576
8x8	3	232.574	254.969	163.594	176.516
12x12	3	231.938	254.379	163.593	176.609
8x8	7	232.647	255.036	163.849	176.713
8x8	20	232.665	255.052	163.909	176.760
Exact:		245.941	245.942	145.339	145.377

Table 3. Predicted displacements and natural frequencies of <u>Active</u> [Ti/PZT-4] cylindrical ring with 100cos2θ Volts applied on the piezoelectric layer.

	Mesh Density						Heyliger et al. (1996) (16x2,N=5)
	5x1	10x1	15x1	20x1	15x2	15x4	
Radial Displacement at Center (mm)							
$w(\theta=0)$	0.0318	0.0976	0.1103	0.1130	0.1084	0.1065	0.1112
$w(\theta=90)$	-0.0318	-0.0976	-0.1103	-0.1130	-0.1084	-0.1065	-0.1112
Natural Frequencies (Hz)							
f_1	57.98	33.01	31.06	30.68	30.96	30.88	31.27
f_2	258.39	174.00	167.64	166.27	167.11	166.68	170.42
f_3	640.39	418.22	399.73	395.23	398.67	397.70	407.29
f_4	1250.39	776.09	730.57	718.47	728.73	726.98	745.21
f_5	2093.49	1263.63	1166.20	1139.05	1163.49	1160.68	1190.48

Table 4. Predicted displacements and natural frequencies of <u>Sensory</u> [Ti/PZT-4] cylindrical ring with a radial line force $F_\zeta = 656$ N/m applied at $\theta = 90°$.

	Mesh Density						Heyliger et al. (1996) (16x2,N=5)
	5x1	10x1	15x1	20x1	15x2	15x4	
Radial Displacement at Center (mm)							
$w(\theta=0)$	-1.004	-2.960	-3.312	-3.387	-3.348	-3.387	-3.750
$w(\theta=90)$	1.128	3.233	3.607	3.687	3.647	3.687	4.083
Electric Potential at Center (V)							
$\phi^F(\theta=0)$	68.90	231.80	266.60	274.60	285.30	284.40	N/A
$\phi^F(\theta=90)$	-107.50	-361.30	-428.80	-453.10	-458.30	-457.70	N/A
Natural Frequencies (Hz)							
f_1	58.83	34.51	32.66	32.28	32.48	32.31	32.60
f_2	264.06	182.15	176.07	174.76	175.19	174.35	175.11
f_3	654.90	437.21	419.13	414.72	417.29	415.35	417.92
f_4	1278.99	811.45	766.07	754.85	762.27	758.54	763.94
f_5	2132.06	1320.94	1223.55	1196.25	1217.60	1211.25	1220.01

27
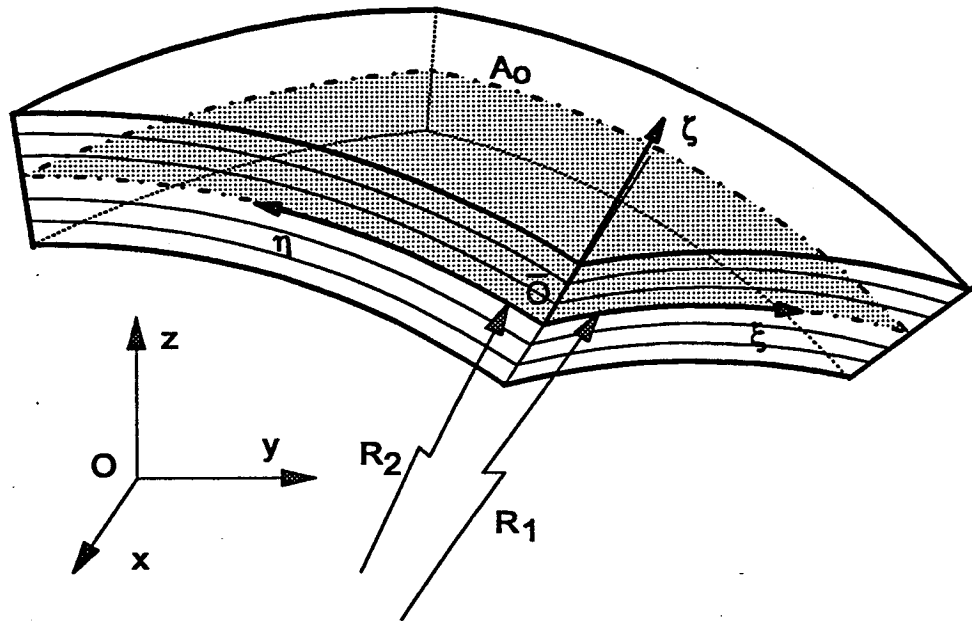
Figure 1.— Curvilinear piezoelectric laminate and coordinate systems.

LAMINATE

Piezoelectric
Layers

Electric potential

Displacements

ϕ^N
ϕ^{N-1}
ϕ^j
ϕ^{j-1}
ϕ^2
ϕ^1

ϕ^N
ϕ^{N-1}

ϕ^j
ϕ^{j-1}

ϕ^2
ϕ^1

ζ

u

u^o

(a) Smart Laminate

(b) Piezoelectric Shell Laminate theory assumptions
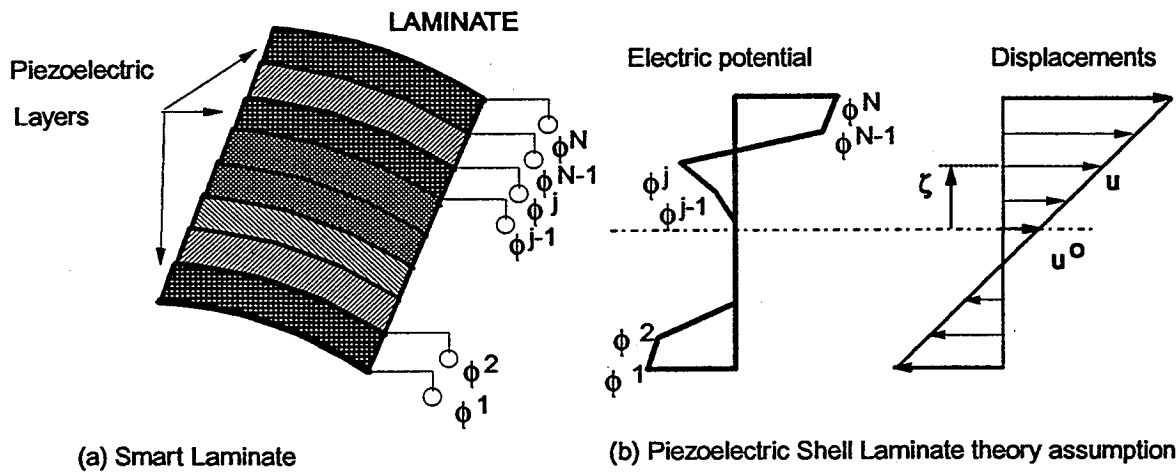
Figure 2.— Typical piezoelectric laminate configuration . (a) Concept ; (b) Assumed through-the-thickness displacement and electric potential fields.
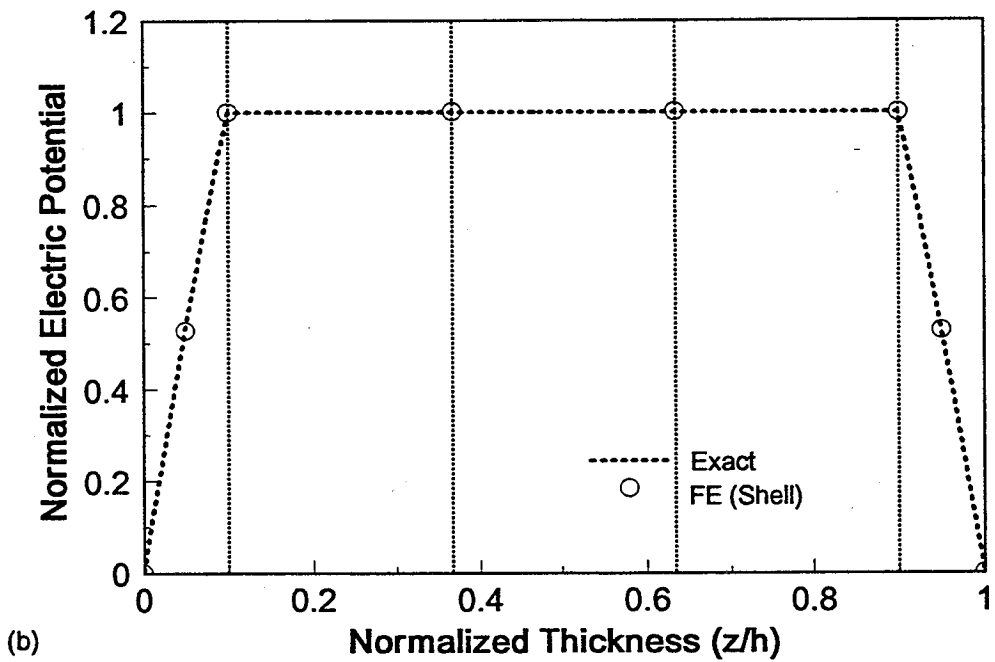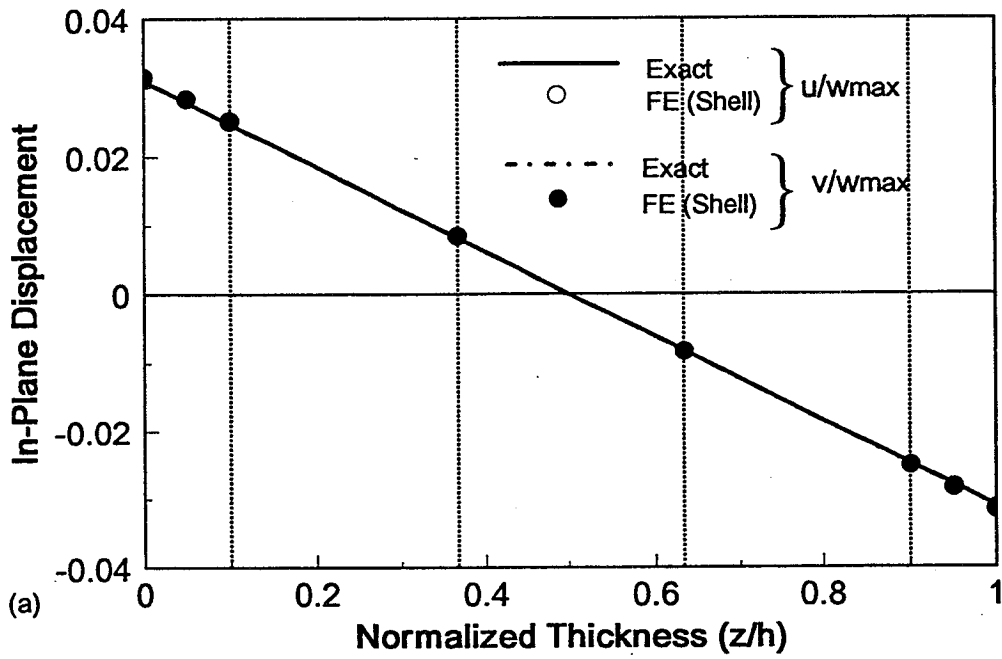
Figure 3.— Through-the-thickness modal displacement and electric potential distributions for a thin [p/0/90/0/p] plate (a/h=50). Fundamental mode.
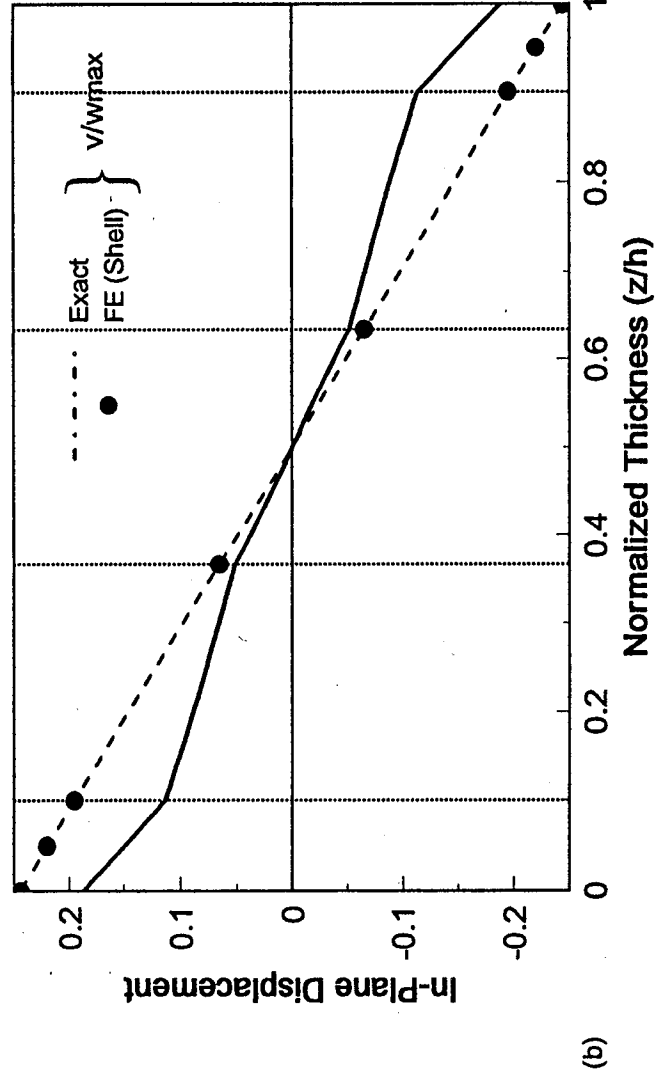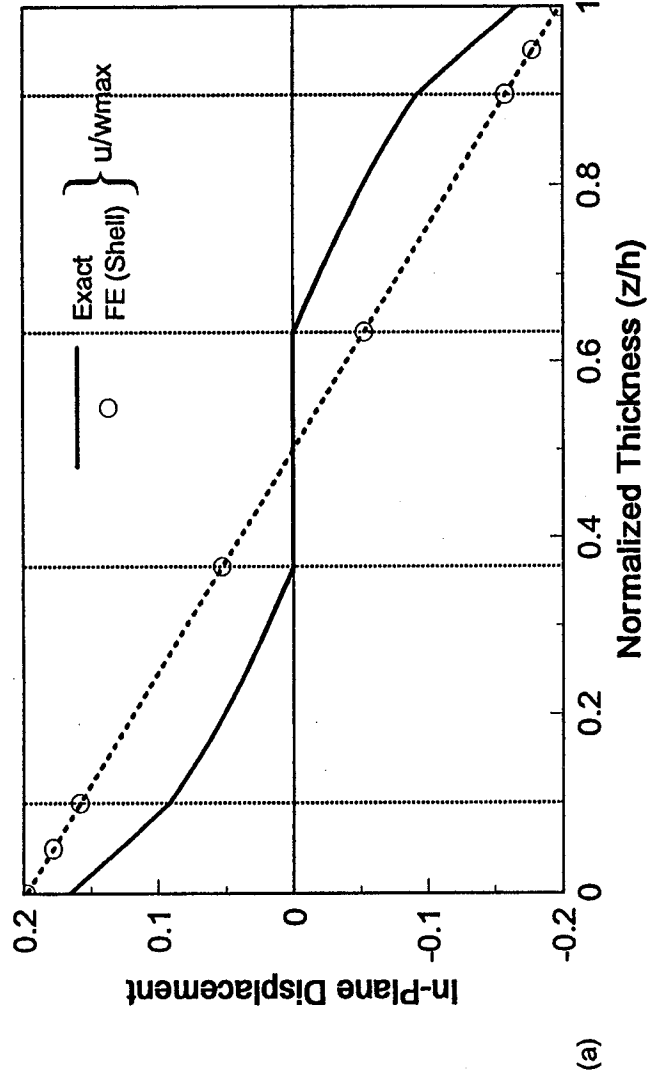
Figure 4.— Through-the-thickness modal displacement and electric potential distributions for a thick [p/0/90/0/p] plate (a/h=4). Fundamental mode.

31
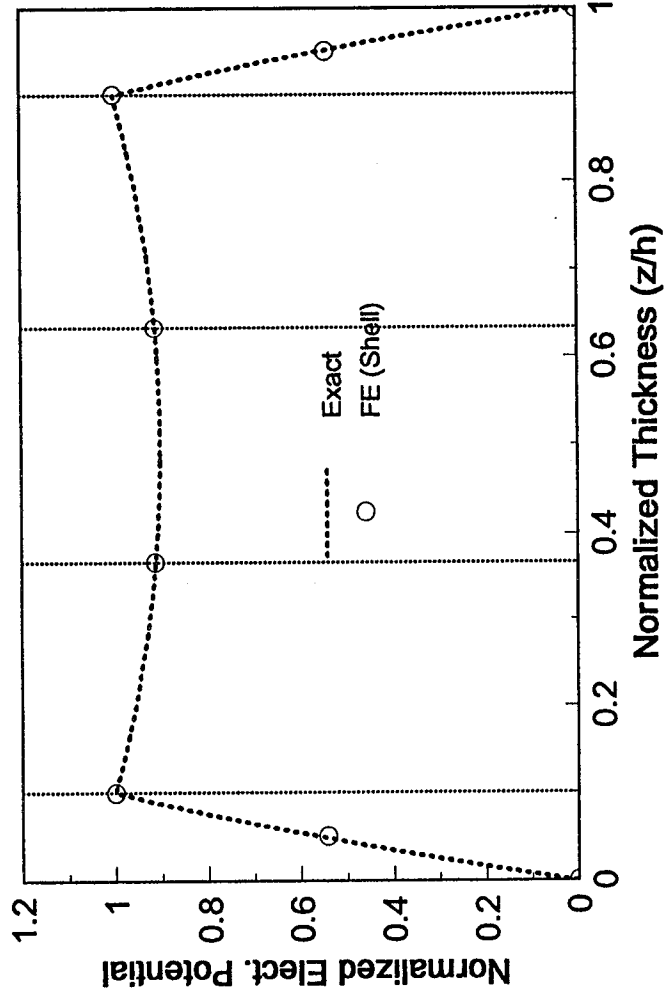
Figure 4.— (Continued)

(c)

32
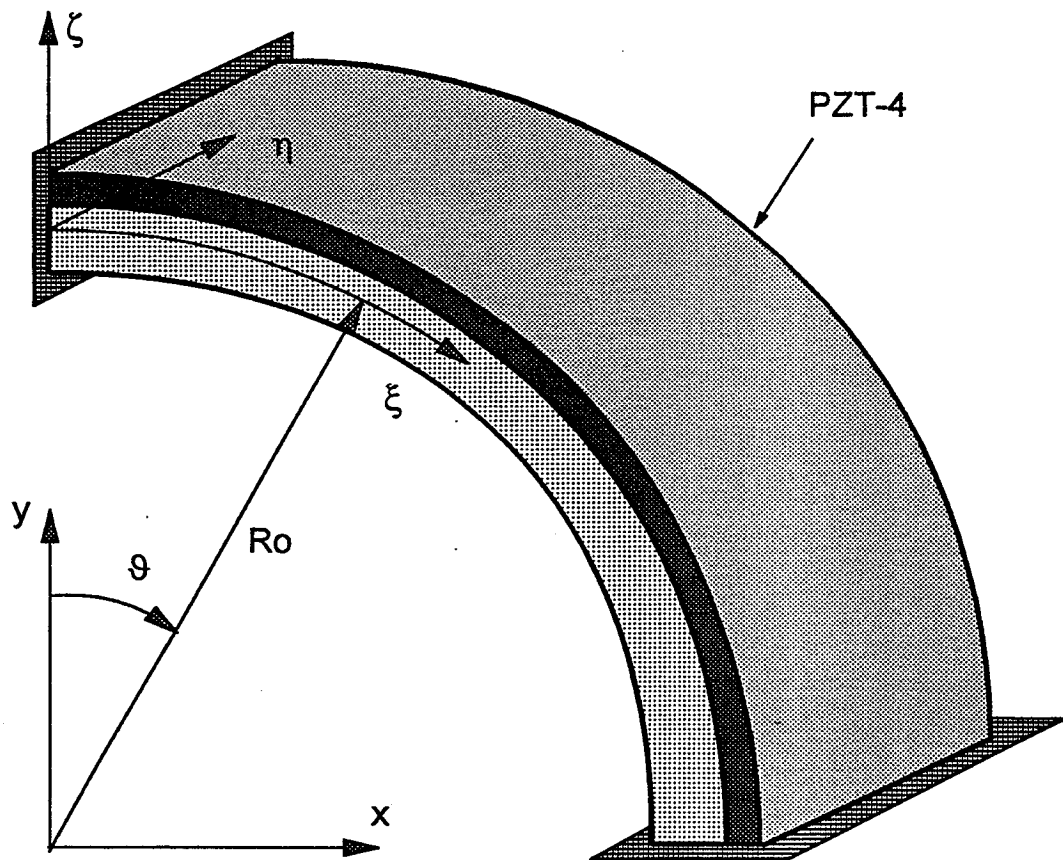
Figure 5.— Quarter model of the cylindrical ring with an attached piezoceramic layer.

Ti/PZT-4 Ring

100 cos2t Volts applied

15x2 mesh, 1/4 model
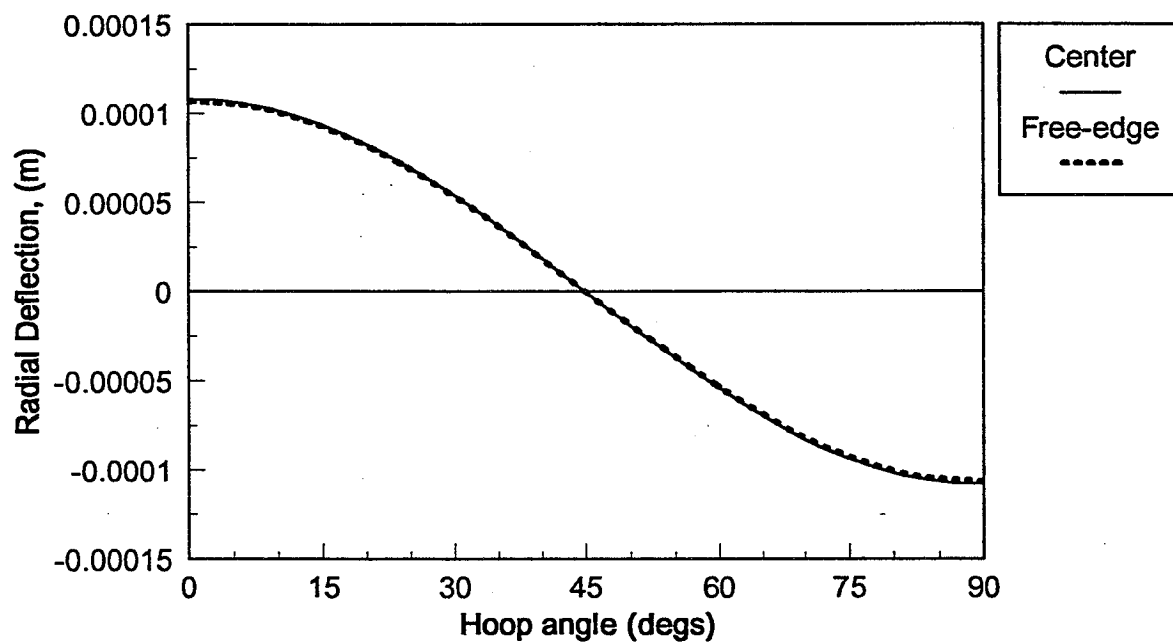
Figure 6.— Actively induced radial deflection of the cylindrical ring with 100cos2θ Volts sinusoidal electric potential applied on the piezoelectric actuator.
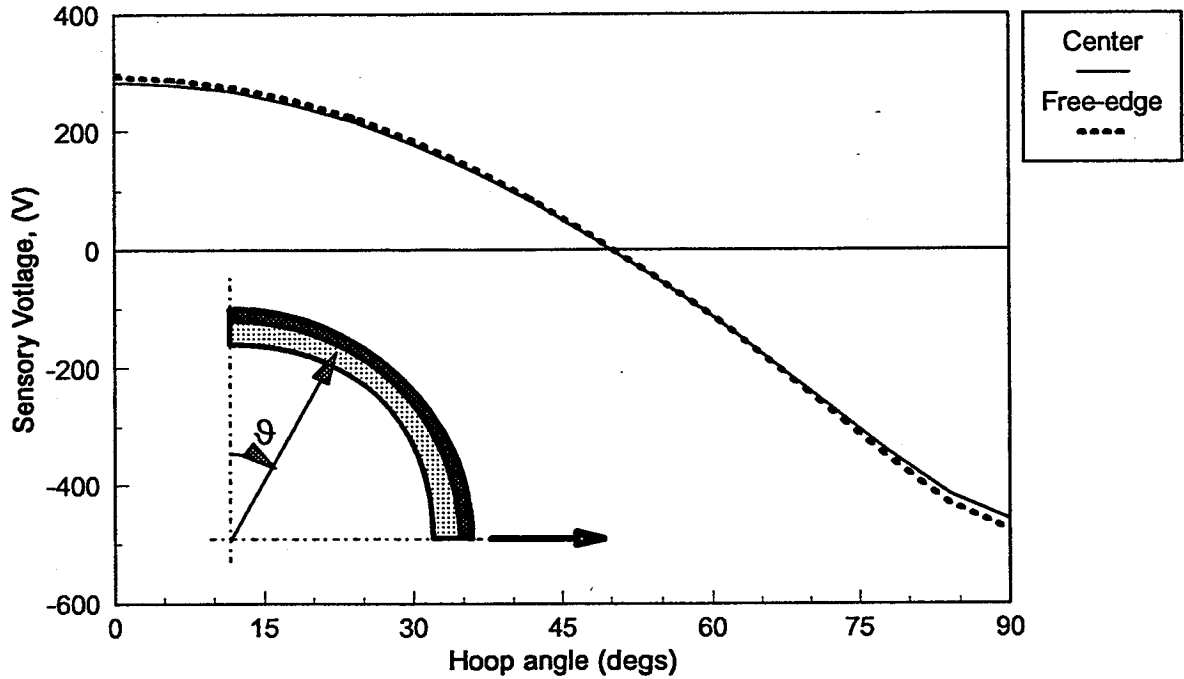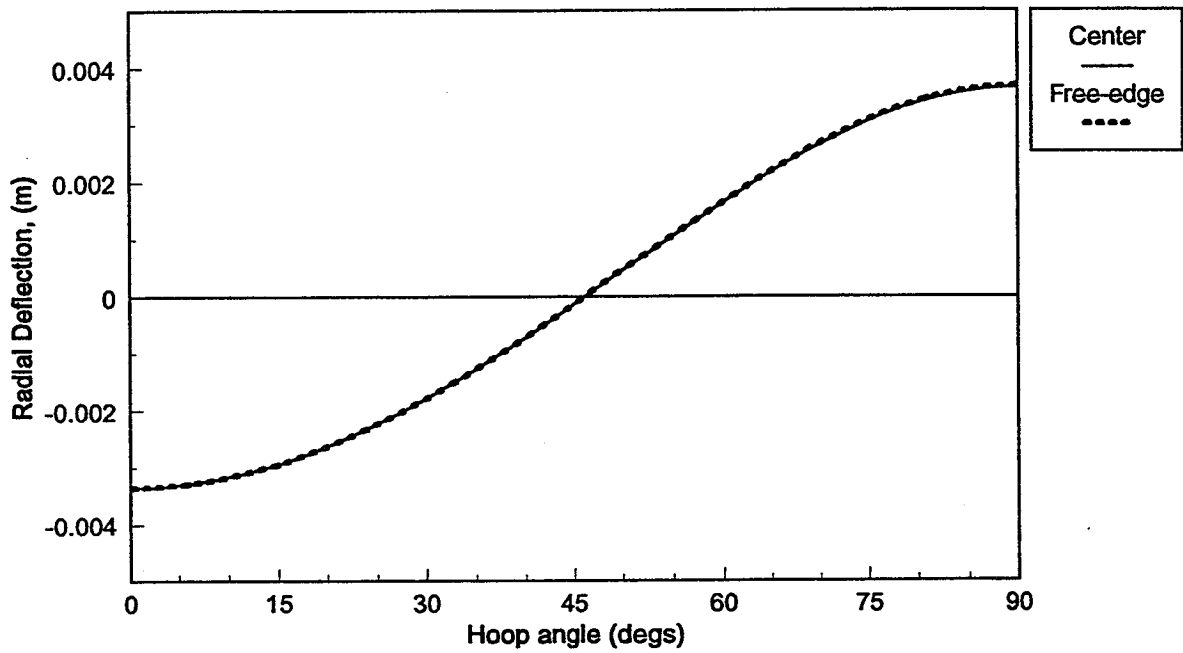
Figure 7.— Radial deflection and corresponding sensory electric potential of the cylindrical ring with a radial line load of 656 N/m applied at θ=90°.

Figure 8.— Semi-circular cantilever shell with 8 surface-bonded cylindrical piezoceramic patches. (a) Geometry; (b) finite element mesh.
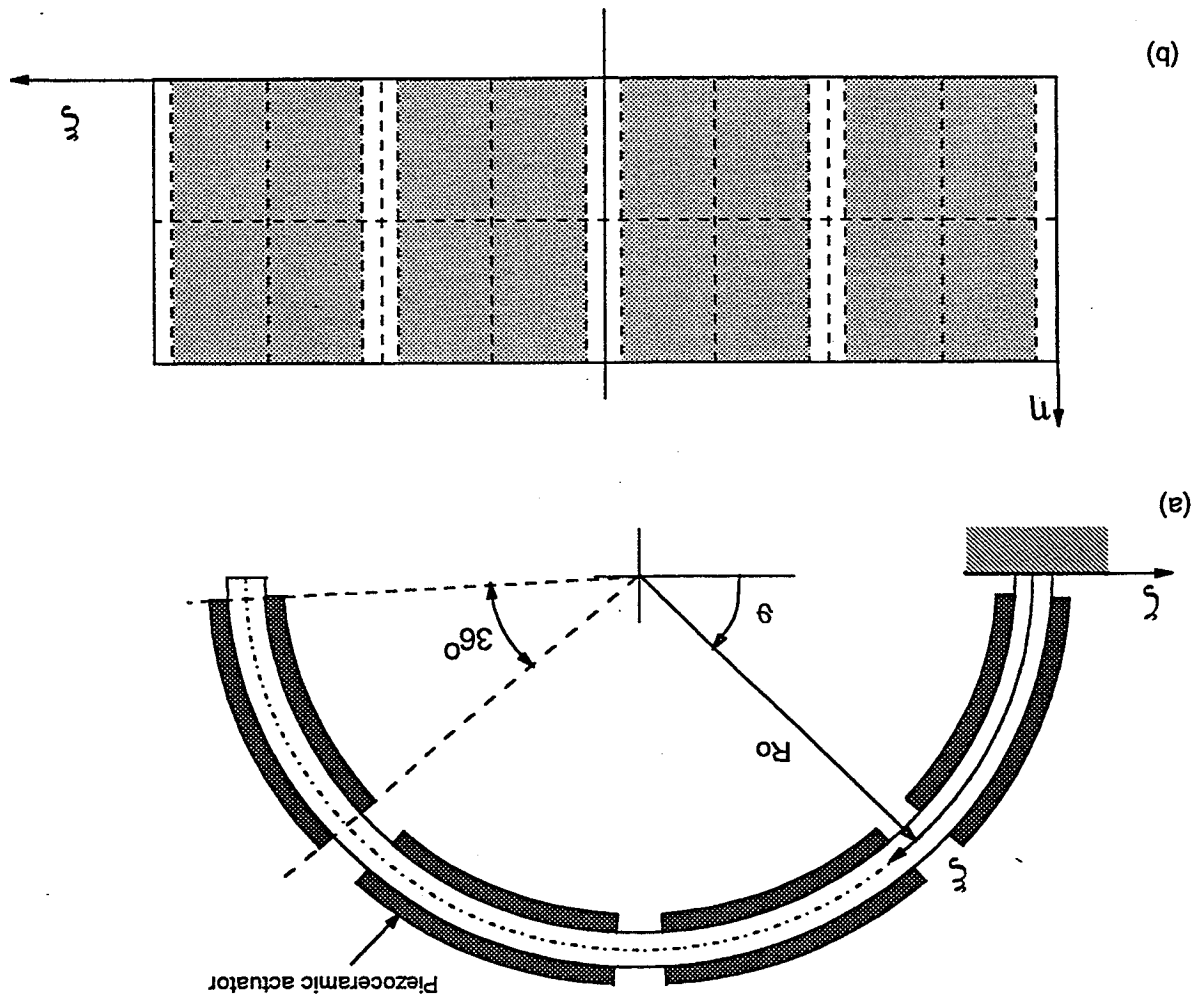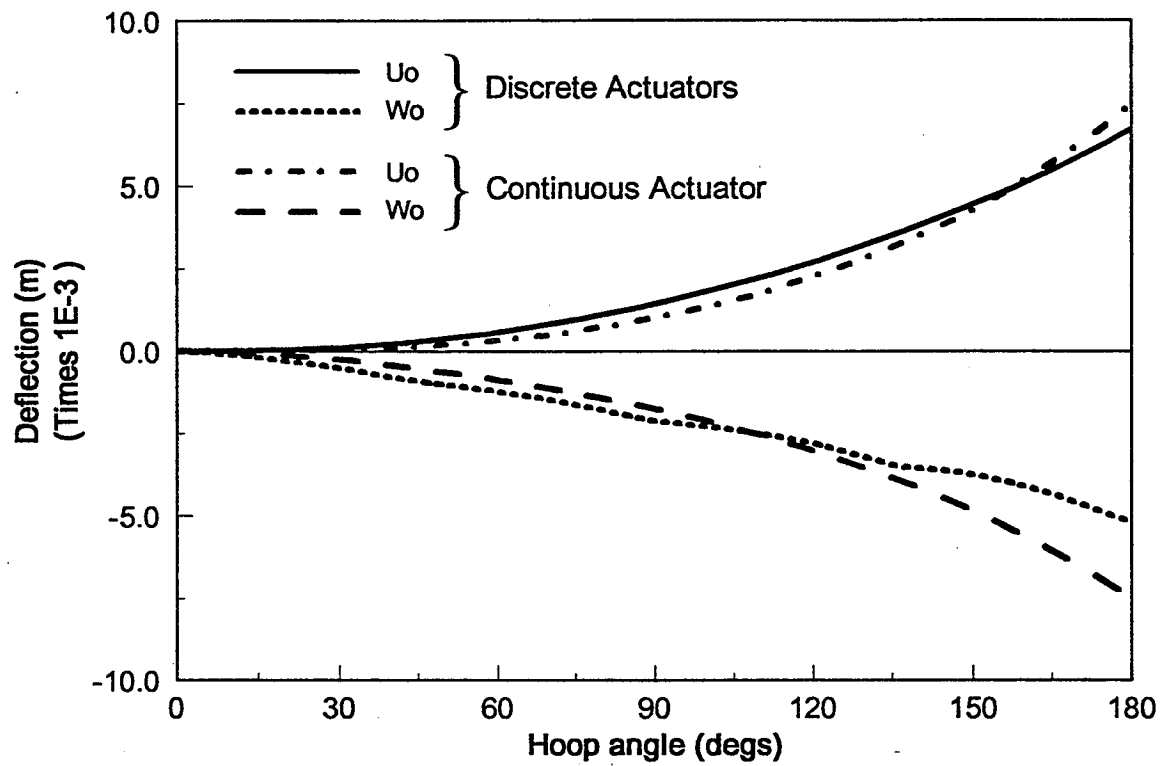
Figure 9.— Active radial and circumferencial deflections of the semi-circular cantilever shell with 100 Volts applied on each piezoelectric patch.
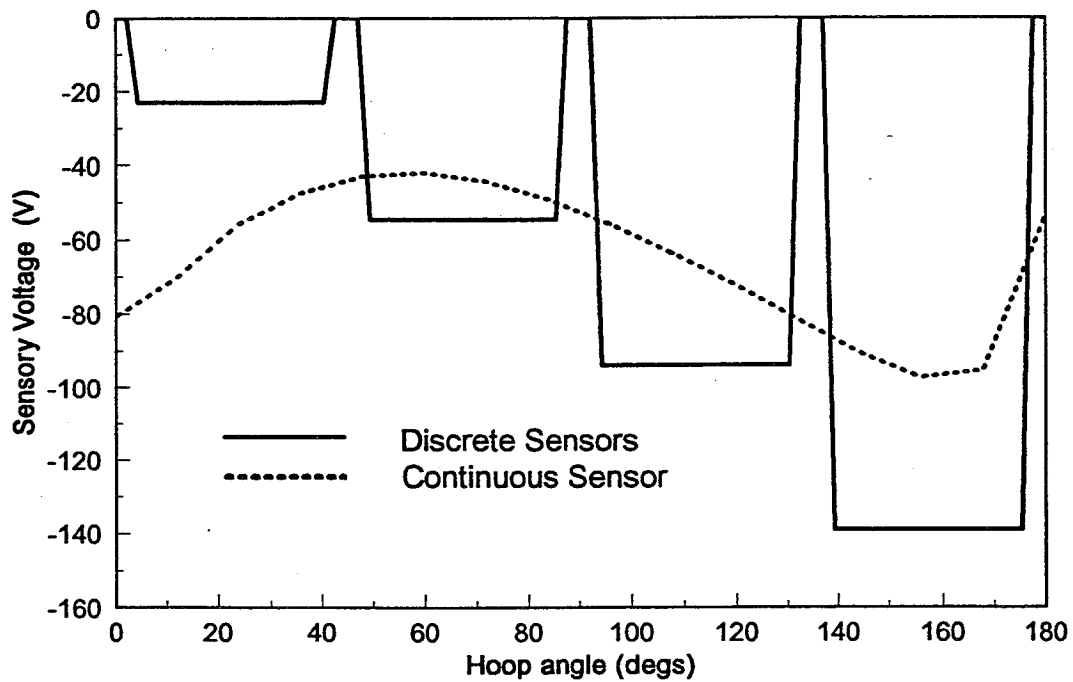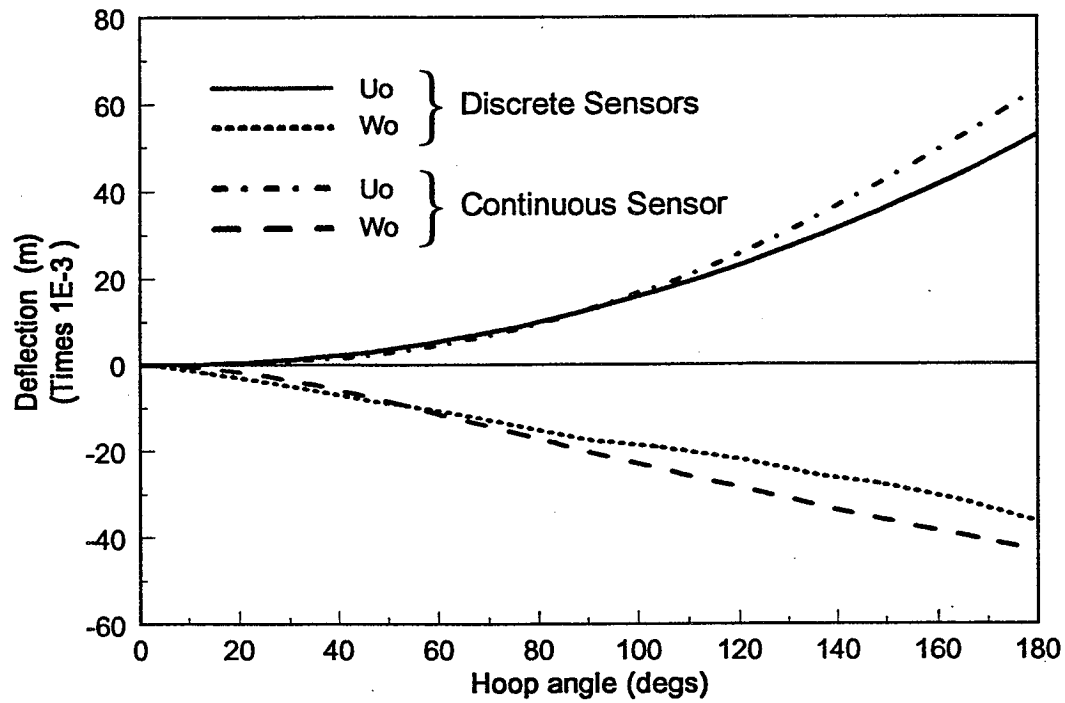
Figure 10.— Radial and circumferencial deflections and corresponding sensory electric potential of the semi-circular cantilever shell with a circumferencial line load $F_\xi = 656$ N/m applied along the free-end.

REPORT DOCUMENTATION PAGE

Public reporting burden for this collection of information is estimated to average 1 hour per response, including the time for reviewing instructions, searching existing data sources, gathering and maintaining the data needed, and completing and reviewing the collection of information. Send comments regarding this burden estimate or any other aspect of this collection of information, including suggestions for reducing this burden, to Washington Headquarters Services, Directorate for Information Operations and Reports, 1215 Jefferson Davis Highway, Suite 1204, Arlington, VA 22202-4302, and to the Office of Management and Budget, Paperwork Reduction Project (0704-0188), Washington, DC 20503.

1. AGENCY USE ONLY (Leave blank)	2. REPORT DATE	3. REPORT TYPE AND DATES COVERED
	June 1996	Final Contractor Report

4. TITLE AND SUBTITLE

Coupled Mixed-Field Laminate Theory and Finite Element for Smart Piezoelectric Composite Shell Structures

6. AUTHOR(S)

Dimitris A. Saravanos

5. FUNDING NUMBERS

WU–505–63–5B
C–NCC3–391

7. PERFORMING ORGANIZATION NAME(S) AND ADDRESS(ES)

Ohio Aerospace Institute
21000 Brookpark Road
Cleveland, Ohio 44135

8. PERFORMING ORGANIZATION REPORT NUMBER

E–10276

9. SPONSORING/MONITORING AGENCY NAME(S) AND ADDRESS(ES)

National Aeronautics and Space Administration
Lewis Research Center
Cleveland, Ohio 44135–3191

10. SPONSORING/MONITORING AGENCY REPORT NUMBER

NASA CR–198490

11. SUPPLEMENTARY NOTES

Project manager, Dale Hopkins, Structures Division, NASA Lewis Research Center, organization code 5210, (216) 433–3211.

12a. DISTRIBUTION/AVAILABILITY STATEMENT

Unclassified - Unlimited
Subject Category 39

This publication is available from the NASA Center for AeroSpace Information, (301) 621–0390.

12b. DISTRIBUTION CODE

13. ABSTRACT (Maximum 200 words)

Mechanics for the analysis of laminated composite shells with piezoelectric actuators and sensors are presented. A new mixed-field laminate theory for piezoelectric shells is formulated in curvilinear coordinates which combines single-layer assumptions for the displacements and a layerwise representation for the electric potential. The resultant coupled governing equations for curvilinear piezoelectric laminates are described. Structural mechanics are subsequently developed and an 8-node finite-element is formulated for the static and dynamic analysis of adaptive composite structures of general laminations containing piezoelectric layers. Evaluations of the method and comparisons with reported results are presented for laminated piezoelectric-composite plates, a closed cylindrical shell with a continuous piezoceramic layer and a laminated composite semi-circular cantilever shell with discrete cylindrical piezoelectric actuators and/or sensors.

14. SUBJECT TERMS

Composite materials; Laminates; Piezoelectricity; Smart structures; Structures; Finite element method; Sensors; Actuators; Shells; Shell theory

15. NUMBER OF PAGES

40

16. PRICE CODE

A03

17. SECURITY CLASSIFICATION OF REPORT	18. SECURITY CLASSIFICATION OF THIS PAGE	19. SECURITY CLASSIFICATION OF ABSTRACT	20. LIMITATION OF ABSTRACT
Unclassified	Unclassified	Unclassified	

National Aeronautics and
Space Administration

Lewis Research Center
21000 Brookpark Rd.
Cleveland, OH 44135-3191